Article

Antibiotics treatment modulates microglia-synapses interaction through CX3CL1/CX3CR1 axis

Federica Cordella[1,2#], Caterina Sanchini[1,2#], Maria Rosito[2#*], Laura Ferrucci[1], Natalia Pediconi[2], Barbara Cortese[3], Francesca Guerrieri[4], Giuseppe Rubens Pascucci[4], Fabrizio Antonangeli[5§], Giovanna Peruzzi[2], Maria Giubettini[6], Bernadette Basilico[1†], Francesca Pagani[2], Alfonso Grimaldi[2], Giuseppina D'Alessandro[1,7], Cristina Limatola[1,7], Davide Ragozzino[1,8##] and Silvia Di Angelantonio[1,2##*]

1 Department of Physiology and Pharmacology, Sapienza University, Rome, Italy; federica.cordella@uniroma1.it; caterina.sanchini@uniroma1.it; laura.ferrucci@uniroma1.it; bernadette.basilico@ist.ac.at; pagani.f@hotmail.com; giuseppina.dalessandro@uniroma1.it; cristina.limatola@uniroma1.it; davide.ragozzino@uniroma1.it; silvia.diangelantonio@uniroma1.it;

2 Center for Life Nano- & Neuro- science, Istituto Italiano di Tecnologia, Rome, Italy; maria.rosito@iit.it; natalia.pediconi@iit.it; giovanna.peruzzi@iit.it; alfonso.grimaldi@uniroma2.it; rocco.pizzarelli81@gmail.com;

3 National Research Council-Nanotechnology Institute, 00185 Rome, Italy; barbara.cortese@nanotec.cnr.it

4 Cancer Research Center of Lyon (CRCL), UMR Inserm U1052 / CNRS 5286, Lyon, France; francesca.guerrieri@inserm.fr; giuseppe92312@gmail.com;

5 Department of Molecular Medicine, Sapienza University of Rome, Laboratory Affiliated to Istituto Pasteur Italia - Fondazione Cenci Bolognetti, Rome, Italy; Fabrizio.antonangeli@uniroma1.it;

6 CrestOptics S.p.A., Via di Torre Rossa 66, 00165 Rome, Italy; giubettini@crestoptics.com;

7 IRCCS Neuromed, Via Atinese 18, 86077, Pozzilli, IS, Italy

8 Santa Lucia Foundation (IRCCS Fondazione Santa Lucia), Rome, Italy

†Current address: Institute of Science and Technology (IST) Austria, Klosterneuburg, Austria.

§ Current affiliation: Institute of Molecular Biology and Pathology, National Research Council (CNR), Rome, Italy

* Correspondence: silvia.diangelantonio@uniroma1.it; maria.rosito@iit.it.

Abstract: 'Dysbiosis' of the adult gut microbiota, in response to challenges such as infection, altered diet, stress, and antibiotics treatment has been recently linked to pathological alteration of brain function and behavior. Moreover, gut microbiota composition constantly controls microglia maturation as revealed by morphological observations and gene expression analysis. However, it is unclear whether gut microbiota influences microglia functional properties and crosstalk with neurons, known to shape and modulate synaptic development and function. Here, we investigated how antibiotic mediated alteration of the gut microbiota influences microglial and neuronal functions in adult mice hippocampus. Hippocampal microglia from adult mice treated with oral antibiotics exhibited increased microglia density, altered basal patrolling activity, and impaired process rearrangement in response to damage. Patch clamp recordings at CA3-CA1 synapses revealed that antibiotics treatment alters neuronal functions, reducing spontaneous postsynaptic glutamatergic currents and decreasing synaptic connectivity, without reducing dendritic spines density. The effect of dysbiosis on neuronal functions are mediated by microglia-neuron crosstalk through the CX3CL1-CX3CR1 axis, as antibiotics treatment of CX3CR1 deficient mice, modulates microglia density and processes rearrangement leaving unaltered synaptic function. Together, our findings show that the antibiotics alteration of gut microbiota impairs synaptic efficacy, probably through CX3CL1-CX3CR1 signaling supporting microglia as a major player in in the gut-brain axis, and in particular in the gut microbiota-to-neuron communication pathway.

Keywords: microglia; gut-brain axis; antibiotics; glutamatergic synapses; hippocampus; patch clamp; hippocampal slices.

 doi:10.20944/preprints202108.0225.v1

1. Introduction

The influence of the gut-brain axis in maintaining brain homeostasis has long been appreciated. However, in the past years the role of the microbiota has emerged as one of the key regulators of gut-brain function, leading to the definition of a novel microbiota-gut-brain axis (MGBA; Cryan et al., 2019). This axis, and in particular gut microbiota composition, has been linked to the biological and physiological basis of psychiatric, neurodevelopmental, age-related, and neurodegenerative disorders (Cryan et al., 2019). The microbiota-brain communication encompasses several possible routes, such as the immune system, the tryptophan metabolism, the vagus nerve and the enteric nervous system, involving microbial metabolites such as short-chain fatty acids, branched chain amino acids, and peptidoglycans (Silva et al., 2020). The manipulation of gut microbiota in animal models has become the paramount paradigm to disclose the causative factors linking the microbiota composition to the regulation of neural and cognitive processes. In addition, ongoing clinical trials are investigating the role of MBGA manipulation for the treatment of brain disorders (Clinical trials.gov Identifier: NCT03237078; NCT04366401 studies). During life, many factors can influence microbiota composition, including infection, mode of birth delivery, use of antibiotic (ABX) medications, nutritional supplement, environmental stressors, host genetics and aging. Moreover, the microbiota and its metabolites have been suggested to be involved in the modulation of brain functions, such as emotional behaviors (Foster and McVey Neufeld, 2013) stress-related responsiveness (Bravo et al., 2012), pain (Bercik et al., 2012), and food intake (Alcock et al., 2014). Consequently, alterations of the ‘‘healthy’’ microbiota, referred to as dysbiosis, might drive functional and behavioral changes in animals and humans (Bercik et al., 2011; Fond et al., 2015).

In this context, preclinical studies demonstrated that ABX administration has long-lasting effects on the brain, spinal cord, and the enteric nervous system (Verdù et al., 2005). Indeed, ABX are known to profoundly alter gut microbiota, possibly resulting in detrimental effects on brain function and behavior as memory impairment in object recognition associated with changes in the expression of related signaling molecules (i.e., BDNF, GRIN2B, 5-HT transporter, and NPY) (Desbonnet et al., 2015; Frohlich et al., 2016). Similarly, chronic long-term ABX treatment was found to induce memory deficits and to decrease hippocampal neurogenesis in adult mice (Mohle et al., 2016; Hoban et al., 2016), while acute treatments was ineffective in rats’ early life (O’Mahony et al., 2014). In addition, microbiota depletion due to ABX, has been shown to impact stress-related behaviors, although the mechanism is still not clear (Tochitani et al., 2016; Leclercq et al., 2017; Desbonnet et al., 2015).

Despite the huge amount of data pointing to the role of MGBA in modulating brain functions, there is the need to understand the intricate processes, and the cellular and molecular events involved. A possible mechanism linking MGBA and neuronal functions arises from the data showing that microbiota composition constantly controls microglia maturation (Erny et al., 2015). Indeed, in germ-free (GF) mice microglia display an immature phenotype, which can be observed also after four weeks of an ABX cocktail treatment of adult microbial colonized mice (Enry et al., 2015). The reported microbiota modulation of microglia phenotype may underlie the effect of MGBA on brain function.

Microglia (the CNS tissue macrophages) are crucial not only for the maintenance of brain homeostasis during development and adulthood, but exert a profound effect on neurons, by refining the neuronal network in physiological and pathological condition, both directly through physical contacts or soluble factors release (Wake et al., 2009; Tremblay et al 2010; Eyo and Wu, 2013) and indirectly, modulating astrocytic beneficial or detrimental activity (Liddelow et al.,2017). One of the key elements in the microglia-neuron crosstalk deeply linked to the synaptic refinement and modulation is the CX3CL1/CX3CR1 axis. Indeed, the disruption of this neuron-microglia signaling causes several alterations in brain connectivity (Zhan et al., 2014) and cognitive functions (Rogers et al., 2011) associated with an impairment in glutamatergic synaptic transmission (Paolicelli et al., 2011; Hoshiko et al., 2012; Zhan et al., 2014; Basilico et al., 2019; Maggi et al., 2011; Rogers et al., 2011). These effects have been generally ascribed to the roles exerted

Preprints (www.preprints.org) | NOT PEER-REVIEWED | Posted: 10 August 2021 doi:10.20944/preprints202108.0225.v1

by microglia during brain development, due to the ability of these cells to foster synaptic pruning (Paolicelli et al., 2011), likely by contacting and phagocyting synaptic elements (Tremblay et al., 2010; Schafer et al., 2012; Weinhard et al., 2018).

Given the impact of microbiota composition on microglia signature, and the role of microglia in tuning synaptic transmission, we explored the possibility that microglia, orchestrating the bidirectional crosstalk between the gut and the brain, might be the missing key element in the MGBA modulation of neuronal functions. For this purpose we altered gut microbiota composition treating mice with two non-absorbable ABX, and we evaluated the impact of two weeks of treatment on microglia and synaptic function. We demonstrated that ABX treatment profoundly affects the ability of microglia in monitoring brain parenchyma homeostasis and impairs the efficacy of hippocampal glutamatergic synaptic transmission. In addition, we showed that ABX did not alters glutamatergic function in CX3CR1 deficient mice, highlighting the involvement of the neuron to microglia CX3CL1/CR3CR1 axis in the microbiota-to-neuron communication pathway.

2. Materials and Methods

2.1 Animals

All the procedures using laboratory animals were in accordance with the Italian and European guidelines and were approved by the Italian Ministry of Health in accordance with the guidelines on the ethical use of animals from the European Communities Council Directive of September 20, 2010 (2010/63/UE). All efforts were made to minimize suffering and number of animals used. Mice were housed in standard cages in a group of maximum 5 animals, with light-dark cycles of 12h at 22±2° C. Mice were divided into two experimental groups, control (CTRL) and antibiotic-treated (ABX). Both groups had sterile food and water ad libitum. Gentamicin (Gibco 15750037) and Vancomycin (Sigma V2002-1G), 0.5 mg/ml were administered starting from P28 for two weeks, 3 times a week, using sterile water feeders in a mix containing 50% sterile water and 50% sterile water plus sugar. CTRL mice received only water solution (50% sterile water and 50% sterile water plus sugar) for two weeks. The ABX treatment was performed as in D'Alessandro et al., 2020 in the same animal facility, and with the same conditions. Mice were sacrificed at P40. For electrophysiological and time lapse recordings, Cx3cr1gfp/+ and Cx3cr1gfp/gfp mice were used. Wild type C57BL-6J were purchased from Charles River and used for Nanostring and rt-PCR analysis. Thy1::gfp mice were used for spine density analysis. All experiments were performed on male mice.

2.2 Electrophysiological recordings

Acute hippocampal slices were obtained from Cx3cr1gfp/+ and Cx3cr1gfp/gfp mice sacrificed at P40. Mice were decapitated under halothane anaesthesia (Sigma Aldrich, Co., St. Louis, MO). Whole brains were removed from the skull and rapidly immersed for 10 min in ice-cold artificial cerebrospinal fluid (ACSF) containing (in mM): KCl 2.5, CaCl2 2.4, MgCl2 1.2, NaHSO4 1.2, glucose 11, NaHCO3 26 and glycerol 250 (Sigma Aldrich), 300 mOsm. ACSF was continuously oxygenated (95% O2 and 5% CO2) to maintain the physiological pH. Horizontal 250-µm-thick slices were cut at 4°C using a Ted Pella vibratome and placed in a chamber filled with oxygenated ACSF containing (in mM): NaCl 125, KCl 2.5, CaCl2 2, MgCl2 1, NaHSO4 1.2, NaHCO3 26 and glucose 10, 300 mOsm. Before use, slices were left to recover for at least 1h at room temperature (24 ± 1°C). All recordings were performed at room temperature on slices sub-merged in ACSF and perfused with the same solution in the recording chamber. Spontaneous currents (sPSC) and excitatory postsynaptic currents were recorded from CA1 pyramidal neurons at −70 mV, using a patch clamp amplifier (Axopatch 200A, Molecular Devices). Data were filtered at 2 kHz, digitized (10 kHz), acquired using pClamp 10.0 software (Molecular Devices), and analyzed offline using Clampfit10 (Molecular Devices). Patch pipettes (3–5MΩ) were filled with intracellular solution containing (in mM): Cs-methane

Preprints (www.preprints.org) | NOT PEER-REVIEWED | Posted: 10 August 2021 doi:10.20944/preprints202108.0225.v1

sulfonate 135, HEPES 10, MgATP 2, NaGTP 0.3, CaCl2 0.4, MgCl2 2, QX-314 2, and BAPTA 5 (pH adjusted to 7.3 with CsOH). Bicuculline methochloride (10 μM) was added to the extracellular solution to block GABAA receptors. For spontaneous EPSCs recordings, in order to equilibrate chloride reversal potential at −70 mV, we used the following Cl−-adjusted intracellular solution (in mM): Cs-methane sulfonate 135, CsCl 7, HEPES 10, MgATP 2, NaGTP 0.3, MgCl2 2, and BAPTA 5 (pH adjusted to 7.3 with CsOH). Evoked EPSC were induced by electrical stimulation via stimulation electrodes put inside a theta glass tubes filled with external solution ACSF (tip 15–20 μm), positioned onto a manual manipulator connected to the unit of stimulation (Iso-stim A320, WPI) to control the quantity of the current applied to stimulate the presynaptic fibers. The glass tube was placed in the stratum radiatum, to activate the Schaffer collaterals projecting to CA1 neurons. The position of the stimulation electrode was chosen based on fixed coordinates with respect to the recorded neuron (around 80 μm toward CA2). For input/output curves (I/O), Schaffer collaterals were stimulated with currents of increasing intensity (0.1, 0.5, 1, 3, 7, 10 mA), holding the potential at -70 mV, to observe the AMPAR-mediated responses. Each stimulus lasted for 0.1 ms and was given for 6 times, one every 10 seconds. The amplitude of around 6 responses for each stimulation was then averaged to obtain the I/O curve.

Patch clamp recordings of CTRL and ABX microglia, in whole cell configuration, were performed by visually identifying GFP-expressing microglial cells in the CA1 stratum radiatum. Slices were perfused with ACSF containing (in mM): NaCl 125, KCl 2.3, CaCl2 2, MgCl2 1, NaHPO4 1, NaHCO3 26, and glucose 10 (Sigma Aldrich). The ACSF was continuously oxygenated with 95% O2, 5% CO2 to maintain physiological pH. Micropipettes (4–5 MΩ) were usually filled with a solution containing the following composition (in mM): KCl 135, EGTA 0,5, MgCl2 2, CaCl2 0,01, HEPES 10 e Mg-ATP 2 (pH 7.3 adjusted with KOH, osmolarity 290 mOsm; Sigma Aldrich). Voltage-clamp recordings were performed using an AxonMulticlamp 700B (Molecular Devices, LLC, Sunnyvale, CA). Currents were filtered at 2 kHz, digitized (10 kHz) and collected using Clampex 10 (Molecular Devices); the analysis was performed off-line using Clampfit 10 (Molecular Devices). Recordings were performed on deep cells, in order to avoid a potentially activated microglia by the slicing procedure. Moreover, experiments were performed from 1 to 7 h after slicing at room temperature. The current/voltage (I/V) relationship of each cell was determined by applying voltage steps from −170 to +70 mV (V = 10 mV) for 50 ms holding the cell at −70 mV between steps. Resting membrane potential and membrane capacitance were measured at the start of recording. Outward and inward rectifier K+ current amplitude were evaluated after subtraction of the leak current by a linear fit of the I/V curve between −100 and −50 mV. Cells were considered as expressing the outward rectifier K+ current when the I/V relationship showed a rectification above −30 mV and the amplitude measured at 0 mV was at least 10 pA, after leak subtraction; similarly cells showing a small inward rectification below −100 mV were classified as expressing the inward rectifier K+ current when subtracted current amplitude was at least 5 pA at −150 mV.

2.3 Time lapse imaging

The rearrangement of microglia processes towards a local injection of ATP (Davalos et al., 2005) was evaluated on acute hippocampal slices acquiring time-lapse images, after at least 2 hours of recovery. Slices were constantly kept in oxygenated ACSF during all the stages of the experiment at room temperature. Images were acquired every 10 seconds for 50 minutes, (exposure time of 200 ms) through a BX51WI microscope (Olympus Corporation, Tokyo, JP. Objectives: LUMPlanF N 10x/0.10, air, and 40x/0.80, water immersion, Olympus Corporation). GFP was excited at 488 nm with an Optoscan monochromator (Carin Research, Facersham, UK). Light was generated by a xenon lamp Optosource (Cairn Research). A borosilicated glass micropipette was filled with ACSF and Mg-ATP 2 mM (Sigma Aldrich), and moved via a micromanipulator MP-225 (Sutter Instruments, Novato, CA) to reach the core of the field recording, around 50 μm beneath

Preprints (www.preprints.org) | NOT PEER-REVIEWED | Posted: 10 August 2021 doi:10.20944/preprints202108.0225.v1

the surface of the slice. The basal fluorescence was evaluated for 5 minutes, then a small volume of Mg-ATP solution was puffed on the slice via a pneumatic pico-pump (PV820; World Precision Instruments, Inc., Sarasota, FL) with a brief pressure (8 psi; 100 ms). The images were acquired with a camera CCD CoolSnap MYO (Photometrics, Tucson, AZ, USA) and then analyzed with MetaFluor software as fluorescence variation measured into five concentric circular regions (regions of interest, ROI) positioned from the tip of the ATP pipette, with a diameter of 10, 20, 40, 80 and 120 μm. To quantify the signal, the formula (F-F0)/F0 was used, where F0 is the average fluorescence before the ATP application and F is the average fluorescence after the ATP application. To evaluate the effect of ABX treatment on microglia processes recruitment, we determined the increase in fluorescence in concentric regions of interest positioned around the tip of the ATP-containing pipette (Pagani et al., 2015, 2019). Measurements are collected after a short puff of ATP (2 mM, 100 ms) in hippocampal slices from CTRL and ABX treated mice.

2.4 Tracking analysis of Microglia dynamics

Microglia basal motility was observed using an upright microscope (Olympus BX51WI) with a 40x 0.8 NA water immersion objective. Videos for analysis were recorded at room temperature (24–25 °C), on slices perfused with oxygenated ACSF. GFP was excited at 488 nm, with a 150 W lamp and a monochromator. Stack images were acquired for 30 frames at 0.1 frames/sec, using a CoolSnap Myo camera and MetaFluor software (Molecular Devices, Foster City, CA, USA). Microglia dynamics were, thus, tracked using ImageJ processing package Fiji and the tracking plugin MTrackJ, as previously reported (Pagani et al., 2015) Once tracked, a custom-written script, implemented in Matlab, was used for correcting the minimum spatial resolution of the tracks within the acquired image (Basilico et al., 2019).

In brief, tracks were traced and transferred into a new coordinate system in which the origin (x=0, y=0) was set as the starting position of each process. Consequently, the tracks were processed with the Matlab script in order that the distance of each point of tracking was set to the minimum resolution distance between the points (i.e. d=0.61 * wavelength/numerical aperture=0.37 mm). Tracks that endured more than 2 minutes with a distance less than 2d, were excluded. The customized tracks obtained were subsequently analyzed to obtain the displacement, length and instantaneous speed.

2.5 Morphology and microglia density analysis

Cx3cr1$^{gfp/+}$ and cx3cr1$^{gfp/gfp}$ mice were transcardially perfused with PBS and 4% PFA; whole brains were maintained in 4% PFA overnight and then incubated in 30% sucrose PBS solution overnight at 4 °C. Brains were stored at -80°C until sectioning. Frozen brains were cut into 50-μm-thick horizontal slices (Leica cryostat), and stored at 4° until use. Images from Cx3cr1$^{gfp/+}$ and Cx3cr1$^{gfp/gfp}$ mouse slices were acquired through a Nikon Eclipse Ti equipped with X-Light V2 spinning disk (CrestOptics), LDI laser source (89 North) and Prime BSI Scientific CMOS (sCMOS) camera, 6.5 μm pixels (Photometrics) with a 10x/0.25 Plan E air objective and a 60x/1.4 PlanApo l oil objective). Metamorph software version 7.10.2 (Molecular Devices) was used to acquire GFP signal with a step size of 3 μm (for 10x) and 0.1-0.3 μm (for 60x). Representative images of the acquired fields were obtained as a z-projection based on the maximal intensity signal, using ImageJ software. Within each acquired stack, all the cells that appear entire were subjected to the analysis. Microglia density was evaluated by counting the number of cell bodies totally contained within the z-projection taking advantage of the endogenous GFP expression. The obtained number was normalized on the acquired volume in each acquisition field. For microglia morphometrical analysis, all the entirely visible cells inside the acquisition field were

Preprints (www.preprints.org) | NOT PEER-REVIEWED | Posted: 10 August 2021 doi:10.20944/preprints202108.0225.v1

analyzed. Cells were then skeletonized on the binary images, using the ImageJ dedicated plug-in.

2.6 Dendritic spine density analysis

Dendritic spine density analysis in the hippocampal stratum radiatum was performed from 60-µm-thick coronal brain slices of Thy1::gfp perfused mice. Images were acquired through a Nikon Eclipse Ti equipped with X-Light V2 spinning disk (CrestOptics), LDI laser source (89 North) and Prime BSI Scientific CMOS (sCMOS) camera with 6.5 µm pixels (Photometrics), using Metamorph software version 7.10.2. (Molecular Devices) with a 100x PlanApo l oil objective (1.45 numerical aperture). The slices in Z were sliced with a step size of 0.1 µm. Signal deconvolution was applied through Huygens software (Huygens professional, Scientific Volume Imaging).

The analysis was performed on secondary and tertiary dendrites starting from maximum z-projection of the planes containing the dendrite segment of interest (ImageJ software). Four dendritic segments were randomly chosen in the field of view (2 fields per slice, six slices per mice, two mice for each condition). The dendrite was then reconstructed and measured to evaluate neurite spine density using NeuronStudio software (version 0.9.92 64-bit, Computational Neurobiology and Imaging Center Mount Sinai School of Medicine, New York, NY).

2.7 Real time PCR

Total RNA was extracted from hippocampal tissue with the Quick RNA MiniPrep (Zymo Research, Freiburg, DE) and retro transcribed with iScript Reverse Transcription Supermix for Real-time PCR (RT-PCR) (Bio-Rad, Hercules, CA, USA). RT-PCR was carried out using Sybr Green (Biorad) according to the manufacturer's instructions. The PCR protocol consisted of 40 cycles of denaturation at 95°C for 30 s and annealing/extension at 60◦C for 30 s. For quantification analysis the comparative Threshold Cycle (Ct) method was used. The Ct values from each gene were normalized to the Ct value of GAPDH in the same RNA samples. Relative quantification was performed using the $2^{-\Delta\Delta Ct}$ method (Schmittgen and Livak, 2008) and expressed as fold change in arbitrary values. Primer sequences targeted against GAPDH forw: TCG TCC CGT AGA CAA AAT GG, GAPDH rew: TTG AGG TCA ATG AAG GGG TC; P2Y12 forw CCT GTC GTC AGA GAC TAC AAG, P2Y12 rew GGA TTT ACT GCG GAT CTG AAA G; P2Y6 forw ATC AGC TTC CTG CCT TTC C , P2Y6 rew CTG TGA GCC TCT GTA AGA GAG ATC G.

2.8 NanoString nCounter gene expression assay and data analysis.

Hippocampal hemispheres were isolated from CTRL and ABX treated mice. Total RNA was extracted with the Quick RNA MiniPrep (Zymo Research, Freiburg, DE). NanoString nCounter Inflammation panel assays were performed using 50 ng of purified RNA following manufacturer's instructions (NanoString Technologies). Sample preparation and hybridization reactions were performed according to manufacturer's instructions (NanoString Technologies). All hybridization reactions were incubated at 65°C for a minimum of 16 h. Hybridized probes were purified and counted on the nCounter SPRINT Profiler (NanoString Technologies) following the manufacturer's instructions. Data analysis was performed using the nSolver analysis software (NanoString Technologies) (https://www.nanostring. com/products/analysis-software/nsolver) and housekeeping genes were used for data normalization. In order to identify the differentially expressed genes (DEGs), those with an interquartile range (IQR) value that stood under the 10th percentile of the IQR value distribution were discarded from the datasets. The expression levels were compared between groups using the paired Wilcoxon rank-sum test on normalized and log2-transformed data. Genes with p-value < 0.05 and fold change > 1.5 were

 doi:10.20944/preprints202108.0225.v1

considered as DEGs. Data analysis of gene expression value was performed using R (version 3.6.2).

2.10 Statistical analysis

Statistical analysis was performed using SigmaPlot, Prism and Origin 6.0 software. Data were assessed for normal distribution and represented in the figures as mean ± s.e.m. For each figure, n = the number of independent biological replicates. No samples or animals were excluded from the analyses. Quantitative RT–PCR, electrophysiological recordings, and time lapse experiments were replicated at least four times with similar results. Differences among more than two groups with only one variable were assessed using one-way ANOVA with Tukey's or Sidak's post hoc test. Comparisons from nanostring gene analysis were analysed using paired Wilcoxon rank-sum test on normalized and log2-transformed data. Two-way ANOVA with Sidak's post hoc test was used for comparisons of two or more groups with two variables. Significant differences emerging from the above tests are indicated in the figures by *P < 0.05, **P < 0.01, ***P < 0.001, ****P < 0.0001. Notable non-significant differences are indicated in the figures by NS.

3. Results

3.1 ABX treatment increases microglia density in the hippocampus without affecting the expression level of inflammation-related genes.

To assess whether the alteration of intestinal microbiota due to oral treatment with non-absorbable ABX, may impact microglia control of brain parenchyma homeostasis, we treated four-weeks old male Cx3cr1gfp/+ mice with a mix of two non-absorbable antibiotics (ABX: Gentamicin and Vancomycin) in drinking water for two weeks. As recently described in a report from our laboratory, ABX administration resulted in a dysbiosis, with an overall reduction in gut microbiota species diversity and alteration of family abundance in the caeca of treated animals (D'Alessandro et al 2020).

Confocal 3D scans of stratum radiatum of hippocampal slices from control and ABX treated Cx3cr1gfp/+ mice showed increased microglia density in ABX treated mice as the number of microglia cells in tissue volume (Figure 1a, b).

To assess if ABX treatment might affect brain homeostasis, we analyzed the inflammatory state of brain parenchyma by nanocounter gene expression analysis of total hippocampal RNA extracts form 6 control and 6 ABX treated mice and found that on control and ABX hippocampal samples only 107 over the 248 genes within the Inflammation mouse panel were expressed. Among these we did not find any upregulation in transcript expression as shown by the heat map (Figure 1c), thus indicating the absence of an inflammatory state in the hippocampus upon ABX treatment. Moreover, we observed downregulation of Nod1 and Cd86 transcripts, as depicted in the volcano plot (Figure 1d). These results suggest that ABX treatment, while inducing a significant change of microglia density, did not modify inflammation-related gene expression in brain parenchyma.

Preprints (www.preprints.org) | NOT PEER-REVIEWED | Posted: 10 August 2021 doi:10.20944/preprints202108.0225.v1

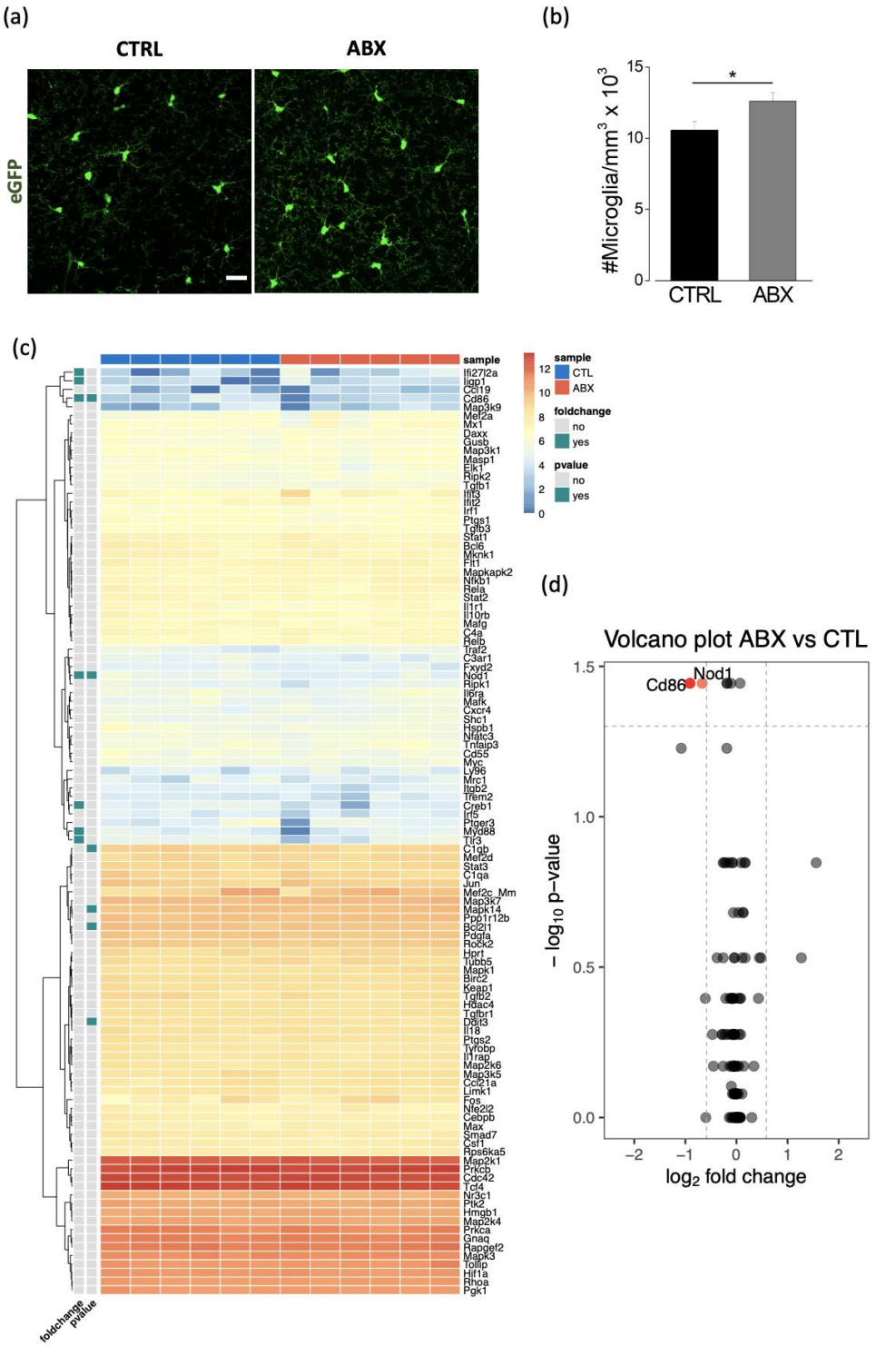

Figure 1. ABX treatment increases microglia density in the hippocampus with no variations in inflammatory gene expression in hippocampal parenchyma. ABX mice display a significant increase of hippocampal microglia density compared to control (CTRL) mice. (a) Representative z-stacks projection showing microglia cells in the hippocampal stratum radiatum of P40 CX3CR1+/GFP CTRL and ABX mice (Green= eGFP, scale bar 20 μm). (b) Bar chart showing microglia mean density in CTRL (10600 ± 600 GFP+ cells/mm3, n= 40 slices/6 mice, black) and ABX mice (12600 ± 600 GFP+ cells/mm3, n=39 slices/6 mice, grey; *p<0.05, Student's T-Test). (c) Heat map of unsupervised hierarchical clustering inflammation genes in CTRL (n=6) and ABX hippocampus samples (n=6) analyzed by NanoString nCounter gene expression assay. Colors in the heatmap indicate log2 counts normalized to housekeeping genes. Note that ABX treatment did not alter the expression of inflammatory related genes in. (d) Volcano plot showing the downregulation of Nod1 and CD86 in ABX hippocampus samples.

3.2 ABX treatment alters microglia functional properties in acute hippocampal slices.

We then analyzed the mopho-functional properties of hippocampal microglia in Cx3cr1gfp/+ mice treated with ABX. First, microglia morphology was assessed in

 doi:10.20944/preprints202108.0225.v1

Confocal 3D scans of stratum radiatum of hippocampal slices from control and ABX treated animals, showing that the treatment- induced increase in density was not related to changes of microglia morphology. Indeed, morphometric parameters of GFP-positive cells in stratum radiatum, obtained by the skeletonization of single microglia cells in confocal 3D scans, were unaffected by ABX treatment (Figure 2 a, b).

In parallel, we analyzed by whole-cell patch clamp recording the electrophysiological properties of visually identified microglial cells of in CA1 stratum radiatum of acute hippocampal slices from Cx3cr1gfp/+ mice. Consistently with the lack of morphological changes, we observed that ABX treatment left unaltered the pattern of voltage activated potassium currents recorded in patch clamped microglia (supplementary Figure 1).

To further investigate the impact of ABX treatment on microglia functions, we focused on patrolling activity, analyzing microglia processes movement in acute hippocampal slices in basal condition and in response to an ATP source. Tracking analysis (Figure 2c) of spontaneous microglia processes movement indicated that in slices from ABX mice, microglia constantly moved their processes with an increased mean velocity (Figure 2d); in addition, measurement of the instantaneous process displacement showed a higher processes displacement in microglia from ABX mice (Figure 2e). This is supported by the instantaneous process displacement plot (Figure 2f), showing that the time dependent increase in radial distance was higher in hippocampal slices from ABX mice.

Preprints (www.preprints.org) | NOT PEER-REVIEWED | Posted: 10 August 2021 doi:10.20944/preprints202108.0225.v1

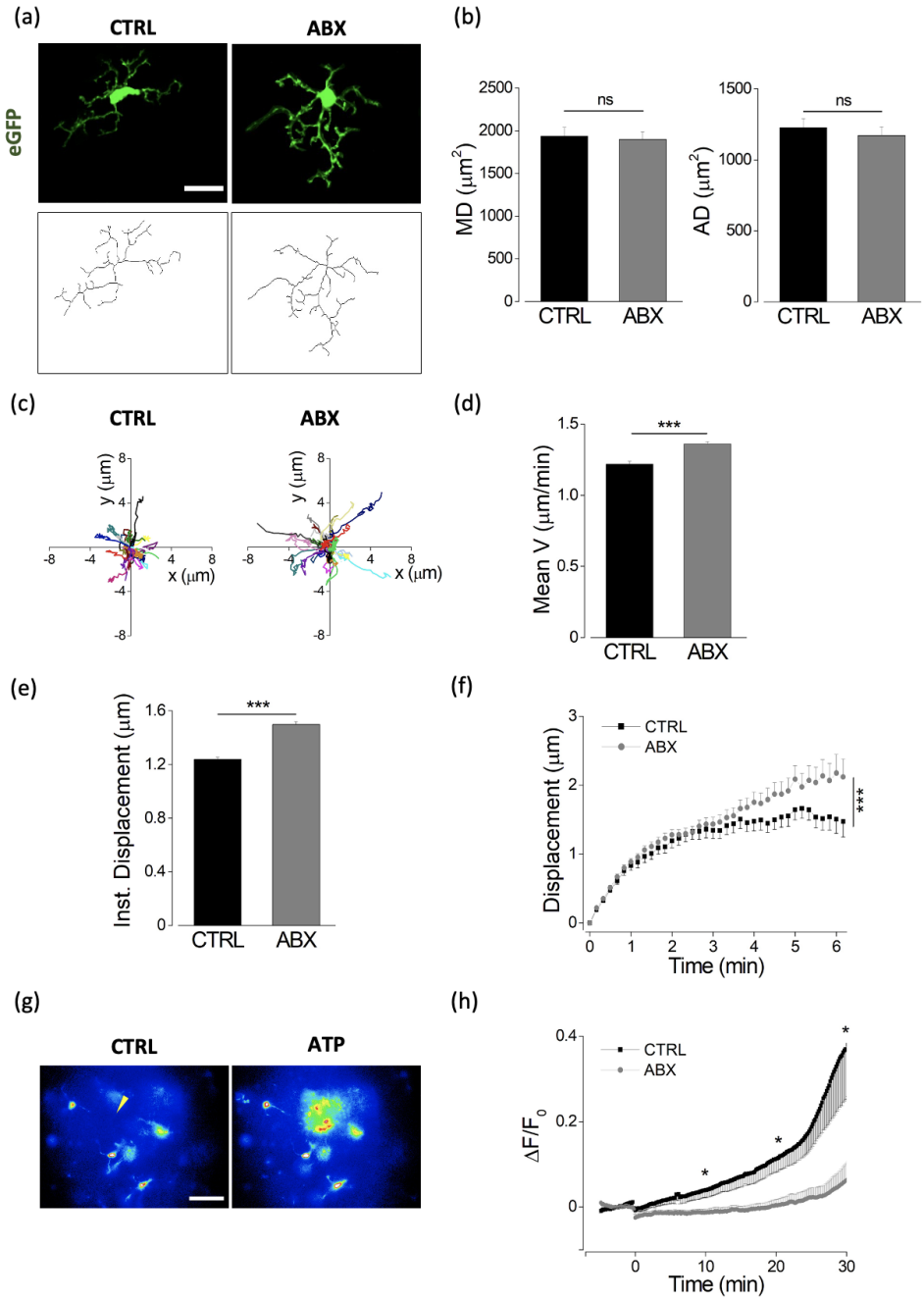

Figure 2: ABX treatment alters microglia functional properties in acute hippocampal slices

Quantitative morphometric analysis of microglia in CTRL and ABX mice. (a) Representative z-stacks projection showing GFP+ microglia (top) and tagged skeleton (bottom) of CTRL and ABX mice. (b) Bar charts of morphometric parameter: mean Arborization Domain in CTRL (62 cells/5 mice) and ABX (66 cells/5 mice; left), and mean Microglial Domain in CTRL (n=54 cells/ 5 mice) and ABX (n=67 cells/5 mice; right). (c) Track analysis of microglia processes basal motility in hippocampal slices from CTRL (left panel) and ABX treated mice, measured by time-lapse fluorescence monitoring in acute hippocampal slices (15 min). Bar graphs representing spontaneous patrolling activity parameters obtained from track analysis: (d) ABX treatment increased mean processes velocity and (e) instantaneous microglia processes displacement compared to CTRL (CTRL n=22 cells/ 4 mice, ABX n=44 cells/ 3 mice; Student t-test ***p<0.001). (f) Plot showing time course of instantaneous radial process displacement in slices from ABX (grey circles) and CTRL (dark squares) mice (Two-way ANOVA ***p<0.001). (g) Representative fields of GFP fluorescence measurements in control and ATP treated slices from Cx3cr1gfp/+ mice. The arrow represents the tip of the ATP puff pipette. 0′ corresponds to ATP application time (Mg-ATP 2 mM, 8 psi, 100 ms). (h) Time course of fluorescence ratio signal (ΔF/F0) measured in a circle (10 µm radius) centered on the tip of the ATP containing pipette, from slices of CTRL and ABX treated CX3CR1+/GFP mice. (CTRL: black, n=12 fields/4 mice and ABX: grey, n=12 fields /4mice; ∗p<0.05, One-way ANOVA at minutes 10, 20 and 30). Note the fluorescence increase in the area around the pipette tip only in control slices. Scale bar: 20 µm.

 doi:10.20944/preprints202108.0225.v1

By time-lapse acquisition in hippocampal slices from Cx3cr1+/gfp mice, we also characterized the ability of microglia to extend processes towards the site of a local ATP application. This procedure typically leads to an increase in the fluorescence level around the pipette tip, due to the extension of microglia processes towards the ATP source. In hippocampal slices from ABX treated mice we observed a significant reduction of the fluorescence increase around the pipette (20 micron radius area; Figure 2g, h) suggesting a reduced ability to respond to ATP.

Real time PCR evaluation of purinergic receptors transcript levels on total hippocampal RNA extracts from control and ABX treated mice revealed increased expression of p2y12 and p2y6 transcripts (see Supplementary Figure 2) in line with what previously reported (D'Alessandro et al 2020).

Taken together, these data indicate that ABX treatment increases microglia density and basal motility, likely favoring the homeostatic patrolling of hippocampal parenchyma. On the other hand, microglia from ABX treated mice are unable to respond to purinergic damage signals.

3.3 ABX treatment impairs hippocampal synaptic transmission.

Considering the deep interplay between neuronal and microglial cells in the modulation of synaptic activity, we wonder whether ABX induced functional changes in microglia could cause changes in synaptic properties. To determine the impact of ABX treatment on hippocampal synaptic transmission, we analyzed excitatory synaptic transmission by patch clamp recordings of CA1 pyramidal neurons in acute slices of control and ABX treated Cx3cr1+/gfp mice (Basilico et al., 2019). First, patch clamp recordings in CA1 pyramidal neurons from mice treated with ABX showed a significant decrease in the amplitude of spontaneous excitatory postsynaptic currents (sEPSC), compared to control, without major effects on sEPSC frequency (Figure 3a, b). Consistently, in ABX-treated mice, excitatory postsynaptic currents (EPSCs) evoked at CA3-CA1 synapses by Schaffer collaterals stimulation displayed strongly reduced amplitudes compared to control ones (Figure 3c, d). This is confirmed by the input/output curve, suggesting that ABX treatment deeply affects CA3-CA1 functional connectivity.

Preprints (www.preprints.org) | NOT PEER-REVIEWED | Posted: 10 August 2021 doi:10.20944/preprints202108.0225.v1

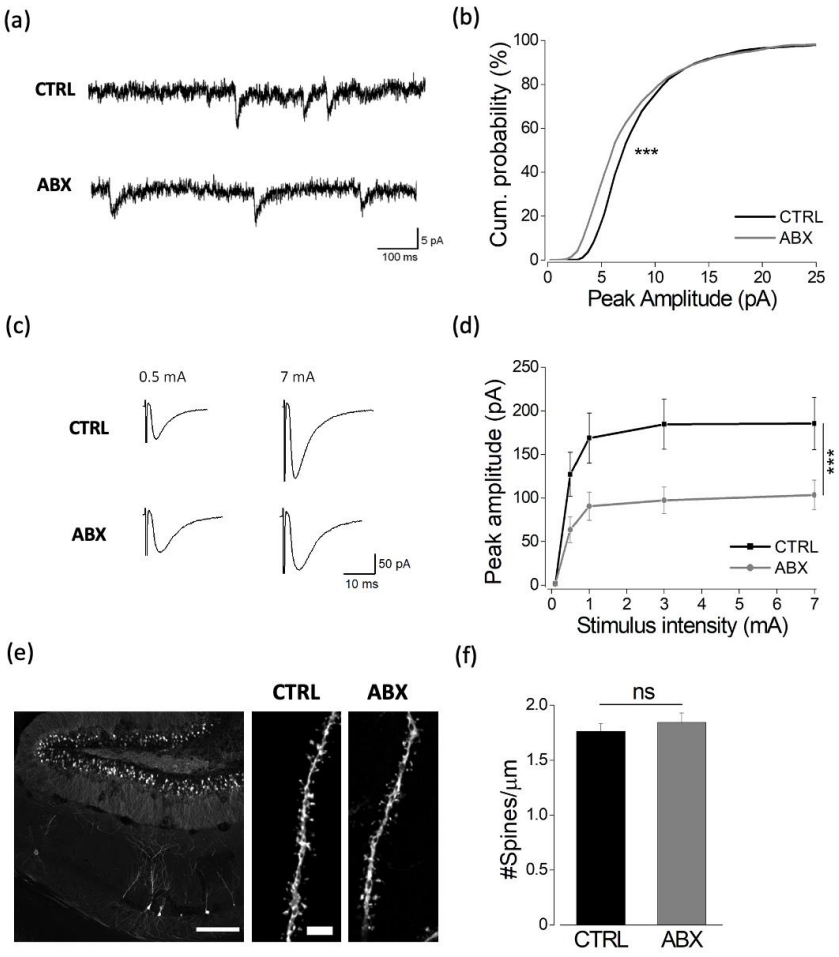

Figure 3. ABX treatment impairs hippocampal glutamatergic synaptic transmission in CX3CR1+/GFPmice . (a) Representative EPSCs recorded at −70 mV from CTRL and ABX mice. (b) Cumulative distribution of sEPSCs recorded from CX3CR1+/GFP CA1 neurons at -70 mV; CTRL (CTRL Mean peak amplitude 8.86 ± 0.3; n=11 cells/4 mice, blue bar) and ABX (ABX Mean peak amplitude 8.05 ± 0.6; n=14 cells/4 mice, orange bar). Note smaller peak amplitudes in ABX compared to CTRL mice (Kolmogorov-Smirnov test, ***p<0.05). (c) Representative traces of spontaneous EPSCs recorded at -70 mV from CTRL and ABX CX3CR1+/GFP CA1 hippocampal neurons in slices from CTRL and ABX mice. (d) Input-output curve of evoked EPSC peak amplitudes at CA3-CA1 synapses recorded at −70 mV from CTRL (n=15 cells/3 mice, black) and ABX mice (n=14 cells/4 mice, grey). Note that in ABX-treated mice, neurons show significantly lower peak amplitudes compared to CTRL (***p<0.001, Two-way ANOVA). (e) Representative confocal images of dendritic segments of CA1 pyramidal neurons in hippocampal slices from CTRL and ABX treated Thy1::GFP mice (scale bar: 200 µm; zoom scale bar: 3 µm). (f) Bar chart representing mean dendritic spine density in the two conditions (CTRL 1.76± 0.07 spines/µm, n=12/2 slices/mice); ABX 1.84 ± 0.08 spines/µm, n=11/2, Student's T-test p=0.45).

To investigate if structural changes may underlie the observed reduced glutamatergic function, we evaluated the dendritic spine density in ABX treated and CTRL Thy-1 GFP mice. Confocal 3D analysis of neuronal CA1 dendritic spine showed that the reduction of glutamatergic transmission was not associated with a change in spine density (Figure 3e, f). These results suggest that ABX treatment affects the synapses functionality, causing a regression and weakening of glutamatergic synaptic transmission between Schaffer collaterals and CA1 pyramidal neurons, thus decreasing functional connectivity.

3.4 Microglia-neuron crosstalk through the CX3CL1/CX3CR1 axis is required for the ABX induced reduction of synaptic transmission.

To ascertain whether the effects induced by ABX treatment on glutamatergic synaptic transmission could be mediated by microglia-neuron crosstalk, we took advantage of a

Preprints (www.preprints.org) | NOT PEER-REVIEWED | Posted: 10 August 2021 doi:10.20944/preprints202108.0225.v1

defective model of microglia-neuron interaction, based on the KO of the fractalkine receptor.

Indeed, in these mice, the lack of neuron microglia crosstalk through the CX3CL1/CX3CR1 axis is known to delay synaptic maturation and connectivity (Basilico et al., 2019; Paolicelli et al., 2011, Hoshiko et al., 2012; Zhan et al., 2014).

It has to be noticed that, while the impairment of synaptic transmission due to the lack of CX3CL1/CX3CR1 signaling develops in the first postnatal weeks (Paolicelli et al., 2011), and perdures in the adult (Basilico et al., 2019; Zhan et al., 2014), the alteration of functional properties of microglia cells, such as ATP processes rearrangement are only transiently present during the second and the third postnatal weeks and recover in the adulthood (Pagani et al., 2015), thus making this model suitable to dissect a possible role of microglia-neuron crosstalk in the ABX induced impairment of glutamatergic synaptic transmission. We thus treated CX3CR1 KO mice with ABX for two weeks. Figure 4 shows that the absence of the CX3CL1/CX3CR1 axis prevented the modulation of synaptic transmission caused by ABX treatment.

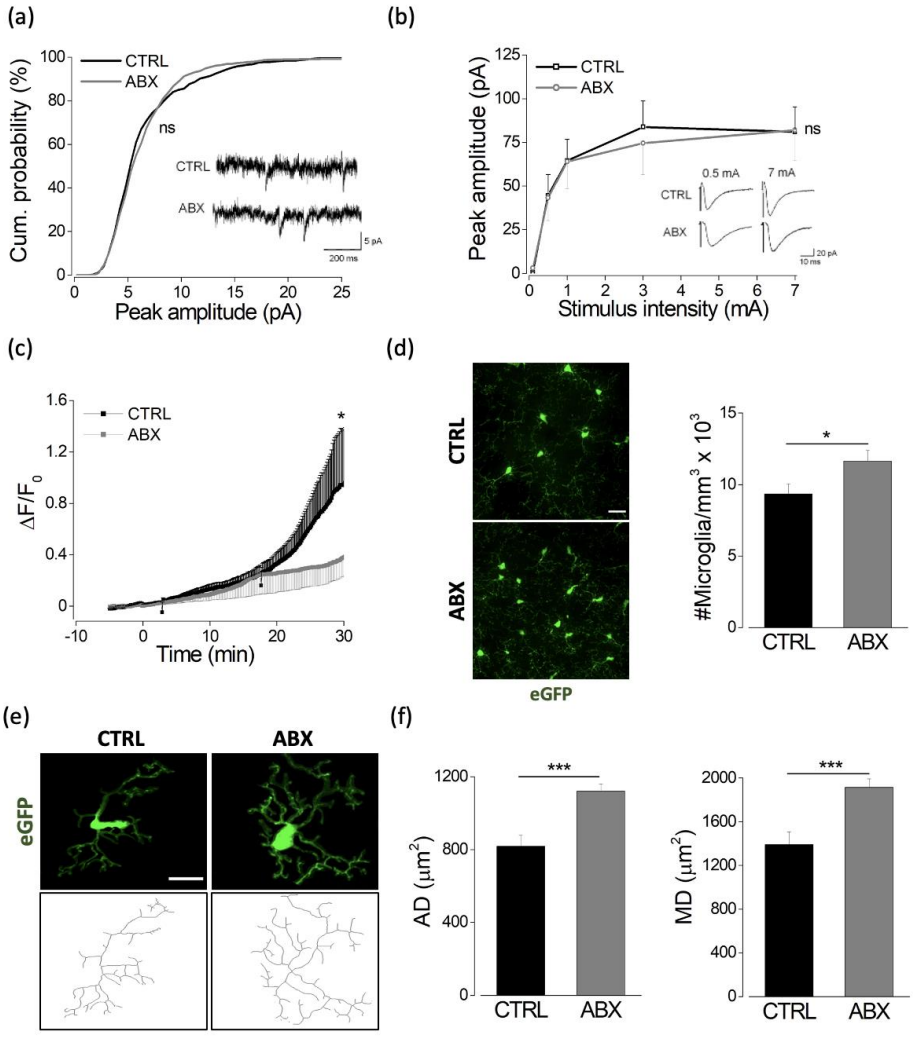

Figure 4: Microglia-neuron crosstalk through the CX3CL1/CX3CR1 axis is required for the ABX induced reduction of synaptic transmission.

(a) Cumulative distribution of sEPSC current amplitude recorded from CX3CR1GFP/GFP CA1 pyramidal neurons (-70 mV holding potential) in slices from CTRL (Mean peak amplitude 6.79 ± 0.1; n=8 cells/3 mice, black) and ABX mice (Mean peak amplitude 6.56 ± 0.1; n=10 cells/3 mice, grey; Kolmogorov-Smirnov test, p=0.18). Inserts: Representative traces of spontaneous EPSCs recorded at -70 mV. (b) Input-output curve of evoked EPSC peak amplitudes at CA3-CA1 synapses recorded at −70 mV from CTRL (n= 12/4, cells/mice, black) and ABX treated CX3CR1GFP/GFP mice (n=9/3, cells/mice, grey; Two-way ANOVA; p=0.86). Inserts: Sample traces of evoked EPSCs in CA1 pyramidal neurons from CTRL and ABX treated CX3CR1GFP/GFP mice. Note that in CX3CR1GFP/GFP mice ABX treatment left unaltered both spontaneous and evoked glutamatergic transmission. (c) Time course of fluorescence ratio (ΔF/F0), measured at ROI10 (10 μm radius centered on the tip of ATP

 doi:10.20944/preprints202108.0225.v1

containing pipette) after 2 mM Mg-ATP solution application (8 psi, 100 ms) on stratum radiatum of acute hippocampal slices from CTRL and ABX CX3CR1GFP/GFP mice (One-way ANOVA $*p<0.05$, at minute 30). Note that ATP-mediated processes rearrangement in untreated mice is similar in both genotypes (One way ANOVA, Dunn's multiple comparison test) (d) Left: Representative z-stacks projection of hippocampal stratum radiatum of Cx3cr1GFP/GFP CTRL and ABX mice (scale bar 20um). Right: bar chart of mean microglia cell density in both conditions (CTRL 9300 ± 700 cells/mm3; n=15 fields/2 mice, black bar; ABX 11700 ±700 cells/mm3; n=18 fields/2 mice, grey bar; Student's T-Test *p value<0.05). (e) Representative z-stacks projection of GFP+ microglia (top) and tagged skeleton (bottom) of CTRL and ABX CX3CR1GFP/GFP mice. (f) Quantitative morphometric analysis of microglia from Cx3cr1GFP/GFP CTRL and ABX mice. Left: bar chart of microglia arborization domain in CTRL (36 cells/10 fields/2mice) and ABX (46 cells/12 fields/2mice; Student's T-Test ***p<0.001); Right: microglial domain in CTRL (n=36cells/10 fields/2 mice) and ABX (n= 46 cells/12 fields/2 mice; Student's T-Test ***p<0.001).

Indeed, ABX treatment did not affect the amplitude as well as the frequency of spontaneous excitatory postsynaptic currents (sEPSC; Figure 4a). Moreover, when we analyzed the CA3-CA1 input/output curve, EPSCs displayed similar amplitudes in control and ABX-treated mice (Figure 4b), suggesting that the CX3CL1/CX3CR1 axis is required for the ABX effect on synaptic transmission.

Conversely, ABX treatment profoundly affected hippocampal microglia, reducing their ability to respond to tissue damage by processes rearrangements (Figure 4, c), increasing microglia density (Figure 4, d) and, noticeably, ramification (Figure 4, e, f).

Altogether, these data indicate that the effect of ABX treatment on CA3-CA1 synaptic function is mediated by the active crosstalk between neurons and microglia mediated through the CX3CL1/CX3CR1 axis, thus pointing to a microbiota-microglia-neuronal axis.

4. Discussion

In this study we explored the impact of oral treatment with non-absorbable ABX on functional properties of hippocampal microglia cells and synaptic transmission. In particular, we analyzed the effect of chronic non absorbable ABX treatment on basal and ATP induced microglia processes motility and glutamatergic synaptic transmission in mouse acute hippocampal slices. Indeed, the modulation of these activities, specifically associated to the resolution of tissue damage and to the activity of neuronal networks may be relevant for the immunomodulatory role of microbiota-gut-brain axis on neuronal functions.

We report that non absorbable ABX treatment affects microglia functions and hippocampal glutamatergic transmission and that the observed effects on synaptic function were mediated by the microglia-neuron crosstalk through the CX3CL1-CX3CR1 axis, as in CX3CR1GFP/GFP mice ABX treatment modulated microglia density and processes rearrangement leaving unaltered synaptic function, making CX3CR1+ cells a major player in in the gut-brain axis, and in particular in the microbiota-immune-neuron communication pathway.

The modulation of microglia patrolling activity by host gut microbes has been demonstrated by a functional assay, monitoring microglia processes movement in basal condition and in response to a local application of ATP, mimicking a tissue damage (Davalos et al.,2005). In particular, in hippocampal slices from ABX treated mice, we observed the alteration of basal patrolling activity and the impairment of ATP induced processes motility. It has been widely reported that under physiological conditions, microglia continuously monitor brain parenchyma, through the extension and retraction of branches (Nimmerjahn et al., 2005). This activity is modified in the presence of an injury, when, following ATP release by damaged neurons, through the activation of purinergic receptors P2Y6 and P2Y12 (Haynes et al., 2006; Takayama et al., 2016), microglia represents

the first response to resolve tissue damage (Davalos et al., 2005; Haynes et al. 2006, Koizumi et al., 2007; Tozaki-Saitoh et al., 2011).

Here, after two weeks of ABX administration the ATP mediated processes rearrangement (Pagani et al., 2015; 2020) is significantly impaired, suggesting a reduced ability of microglia cells to start a rapid response to tissue damage. This effect cannot be ascribed to a down regulation of p2y12 transcript or protein (D'Alessandro et al., 2020), pointing to the involvement of an intermediate amplificatory step (Davalos 2005; Gyoneva 2014) or other control steps of the extracellular ATP degradation or the rearrangement process. However, we cannot exclude a reduction of functionality of ATP receptors.

On the other hand, we observed significant changes in the pattern of basal processes motility in slices from ABX mice. Specifically, we report an increase of processes displacement and mean velocity, thus suggesting a larger scanning territory. Based on these data, we speculate that the ABX treatment could improve the ability of microglia processes to sample the surrounding brain parenchyma. However, these changes were not associated to rearrangement in cell morphology, but only in cell density. This seems to be in contrast with recent reports were in mice born and raised under germ-free (GF) conditions, and in colonized adult SPF treated with a mix of ABX strong enough to eradicate gut bacteria, microglia displayed an immature phenotype, characterized by altered gene expression, increased numbers, and hyper-ramified morphology (Erny 2015, Mezo et al., 2020). It has to be noted, however, that our experimental protocol is based on the administration of two non-absorbable antibiotics for only two weeks, which, as recently reported, did nor eradicate gut bacteria (D'Alessandro et al., 2020). In addition, nanostring analysis of hippocampal extracts did not show changes in the transcript level of inflammatory genes. It has to be noticed that while the downregulation of two over 248 genes prevented a gene ontology analysis, Nod1 and CD86 may play important role on gut brain axis. Indeed, the expression of Nod1 had been recently reported to regulate central and peripheral serotonergic biology, and thus to be related to the proper function of gut–brain axis signaling in mice (Pusceddu et al.,2019). Moreover, decreased CD86 gene expression has been reported in microglia isolated from GF (Erny et al., 2015).

Thus, we speculate that these alterations of brain homeostasis might arise from a change in the pattern of the tissue molecular cues, like signals from gut bacteria, that are necessary for proper microglial homeostasis and functions (Pfeiffer et al., 2016; Kluge et al., 2017; Pagani et al., 2020; Mezo et al., 2020). Possible candidates are SCFA, gut bacteria metabolites that cross the gut barrier, that have been found to be reduced in GF and ABX mice, and to rescue microglia phenotype in GF mice (Erny et al., 2015), moreover, recently it has been described that sodium butyrate and indole-3-propionic acid, both produced by gut microbiota, have potential anti-inflammatory effects on human astrocytes (Garcez et al., 2020).

Although in our experimental conditions ABX treatment does not deplete gut microbiota, the experimental advantage of using ABX to manipulate microbiota is that this represents a tool to model the clinical scenario in humans, with scheduled administration mimicking what millions of people take each year for multiple conditions, allowing us to determine the effect that such treatments may have on the brain functions.

ABX treatment offers much greater temporal flexibility and specificity compared to the GF model of microbiota ablation as ABX can be delivered acutely or chronically at any life stage. Moreover, the appropriate choice of the ABX composition and dosage allows for a greater level of control over the extent of microbiota alteration, from minor perturbations through subtherapeutic doses of a single antibiotic, to entire microbiota ablation by specific ABX cocktail design.

An important consideration in the use of ABX to investigate the MGBA axis is their systemic entering from the gut. Non absorbable ABX [i.e., vancomycin, neomycin, and gentamicin], that do not enter the systemic circulation, can be used to manipulate gut microbiota avoiding any potential systemic and CNS effects and thus allowing the direct assessment of MGBA. Conversely, ABX that can potentially enter the CNS, such as metronidazole and minocycline, can have direct action on brain and behavior (e.g., the reduction of microglia pro-inflammatory mediators by minocycline) (Degroote et al., 2016; Frohlich et al., 2016; Guida et al., 2018).

Notably, we report that the impact of a short ABX treatment (2 weeks) was not confined to microglia cells. Indeed, in ABX mice we found a functional impairment of adult glutamatergic CA3-CA1 synaptic function, as revealed by the reduction of the amplitudes in evoked and spontaneous EPSC and by the apparent regression in synaptic maturation. In particular, we observed a reduced efficacy in CA1 glutamatergic synapses, as shown by the lower AMPA/NMDA ratio (Hsia et al., 1998), and in the postsynaptic sensitivity to the neurotransmitter (reduced sEPSC amplitude in ABX mice), without a structural change in the postsynaptic spine number, pointing to a functional reduction of glutamatergic transmission.

Notably, ABX treatment, while affecting structural and functional properties of microglia, did not produce any significant effect on synaptic properties of mice lacking the fractalkine receptor in microglia (Cx3cr1GFP/GFP mice), a well assessed model of dysfunctional neuron-microglia signaling (Basilico et al., 2019; Paolicelli et al., 2011; Zhan et al.,2014). Thus we can speculate that the ABX induced synaptic dysfunction is dependent on functional microglia neuron interaction, as it is cannot be reproduced where microglia-neuron signaling is already impaired by the lack of CX3CR1/CX3CL1 axis (Paolicelli et al., 2011; Basilico et al., 2019).

Indeed, microglia is known to control synaptic function, using several signaling mechanisms, including regulation of pruning and synaptogenesis (Paolicelli et al., 2011; Parkhurst et al., 2013), release of substances (see Szepesi et al., 2018; Marinelli et al., 2019 for review) or physical contact (Weinhard et al., 2018; Akiyoshi et al., 2018).

5. Conclusions

In conclusion, our study highlights the importance of microglia in mediating the gut-brain axis control of synaptic functioning in the adult brain. ABX-induced microbiota alteration impairs microglia control of brain parenchyma homeostasis, and reduces the efficacy of glutamatergic synaptic transmission. Our results point to a pivotal role of microglia in the MGBA; specifically, the lack of microglia-neuron crosstalk mediated by the CX3CR1/CX3CL1 axis prevented the ABX impairment of synaptic transmission, leaving unaltered the effects on microglia.

Supplementary Materials: The following are available online at www.mdpi.com/xxx/s1, Figure S1: Voltage activated potassium currents in microglia from control and ABX mice. Figure S2: Real Time PCR Analysis of microglia transcripts.

Author Contributions: Conceptualization, S.D.A.; C.L. and D.R.; methodology, G.P; M.R.; A.G; F.G.; G.D.A.; F.P. and F.A. software, B.C.; formal analysis, F.C.; C.S.; L.F.; M.R.; M.G.; investigation, F.C.; C.S.; L.F.; M.R.; M.G.; F.P.; resources, G.D.A. and C.L.; data curation, F.C.; C.S.; M.R.; L.F.; writing—original draft preparation, S.D.A.; M.R.; F.C. and C.S; writing—review and editing, D.R. and S.D.A.; supervision, C.L.; D.R. and S.D.A.; project administration, S.D.A. and D.R.; funding acquisition, D.R. and S.D.A. All authors have read and agreed to the published version of the manuscript.".

Funding: Please add: This research was funded by the CrestOptics-IIT JointLab for Advanced Microscopy (to S.D.A.), the MARBEL Life2020 grant (to S.D.A.), the SynaNet H2020 Program (to C.L.). The authors wish to thank the Center for Life Nano Science Imaging Facility and Cell Sorting

Facility, Istituto Italiano di Tecnologia. This work was partially supported by Sapienza University and Fondazione Istituto Italiano di Tecnologia. F.C., C.S., L.F.,

The APC was funded by Fondazione Istituto Italiano di Tecnologia.

Institutional Review Board Statement: The study was conducted according to the Italian and European guidelines and were approved by the Italian Ministry of Health in accordance with the guidelines on the ethical use of animals from the European Communities Council Directive of September 20, 2010 (2010/63/UE). All efforts were made to minimize suffering and number of animals used.

Acknowledgments: The authors wish to thank the Center for Life Nano Science Imaging Facility and Cell Sorting Facility, Istituto Italiano di Tecnologia.

Conflicts of Interest: The authors declare no conflict of interest. The funders had no role in the design of the study; in the collection, analyses, or interpretation of data; in the writing of the manuscript, or in the decision to publish the results.

References

1. Akiyoshi R, Wake H, Kato D, Horiuchi H, Ono R, Ikegami A, Haruwaka K, Omori T, Tachibana Y, Moorhouse AJ, Nabekura J. Microglia Enhance Synapse Activity to Promote Local Network Synchronization. eNeuro. 2018 Oct 25;5(5):ENEURO.0088-18.2018. doi: 10.1523/ENEURO.0088-18.2018. PMID: 30406198; PMCID: PMC6220592.

2. Alcock J, Maley CC, Aktipis CA. Is eating behavior manipulated by the gastrointestinal microbiota? Evolutionary pressures and potential mechanisms. Bioessays. 2014 Oct;36(10):940-9. doi: 10.1002/bies.201400071. Epub 2014 Aug 8. PMID: 25103109; PMCID: PMC4270213.

3. Anderson MA, Burda JE, Ren Y, Ao Y, O'Shea TM, Kawaguchi R, Coppola G, Khakh BS, Deming TJ, Sofroniew MV. Astrocyte scar formation aids central nervous system axon regeneration. Nature. 2016 Apr 14;532(7598):195-200. doi: 10.1038/nature17623. Epub 2016 Mar 30. PMID: 27027288; PMCID: PMC5243141.

4. Basilico B, Pagani F, Grimaldi A, Cortese B, Di Angelantonio S, Weinhard L, Gross C, Limatola C, Maggi L, Ragozzino D. Microglia shape presynaptic properties at developing glutamatergic synapses. Glia. 2019 Jan;67(1):53-67. doi: 10.1002/glia.23508. Epub 2018 Nov 11. PMID: 30417584.

5. Basilico B., Cortese B., Ratano P., Di Angelantonio S., Ragozzino D. (2019) Time-lapse Whole-field Fluorescence Imaging of Microglia Processes Motility in Acute Mouse Hippocampal Slices and Analysis. Bio-protocol 9(08): e3220. Doi:10.21769/BioProtoc.3220

6. Bercik P, Collins SM, Verdu EF. Microbes and the gut-brain axis. Neurogastroenterol Motil. 2012 May;24(5):405-13. doi: 10.1111/j.1365-2982.2012.01906.x. Epub 2012 Mar 8. PMID: 22404222.

7. Bercik P, Denou E, Collins J, Jackson W, Lu J, Jury J, Deng Y, Blennerhassett P, Macri J, McCoy KD, Verdu EF, Collins SM. The intestinal microbiota affect central levels of brain-derived neurotropic factor and behavior in mice. Gastroenterology. 2011 Aug;141(2):599-609, 609.e1-3. doi: 10.1053/j.gastro.2011.04.052. Epub 2011 Apr 30. PMID: 21683077.

8. Bravo JA, Julio-Pieper M, Forsythe P, Kunze W, Dinan TG, Bienenstock J, Cryan JF. Communication between gastrointestinal bacteria and the nervous system. Curr Opin Pharmacol. 2012 Dec;12(6):667-72. doi: 10.1016/j.coph.2012.09.010. Epub 2012 Oct 4. PMID: 23041079.

9. Cryan JF, O'Riordan KJ, Cowan CSM, Sandhu KV, Bastiaanssen TFS, Boehme M, Codagnone MG, Cussotto S, Fulling C, Golubeva AV, Guzzetta KE, Jaggar M, Long-Smith CM, Lyte JM, Martin JA, Molinero-Perez A, Moloney G, Morelli E, Morillas E, O'Connor R, Cruz-Pereira JS, Peterson VL, Rea K, Ritz NL, Sherwin E, Spichak S, Teichman EM, van de Wouw M, Ventura-Silva AP, Wallace-Fitzsimons SE, Hyland N, Clarke G, Dinan TG. The Microbiota-Gut-Brain Axis. Physiol Rev. 2019 Oct 1;99(4):1877-2013. doi: 10.1152/physrev.00018.2018. PMID: 31460832.

10. D'Alessandro G, Antonangeli F, Marrocco F, Porzia A, Lauro C, Santoni A, Limatola C. Gut microbiota alterations affect glioma growth and innate immune cells involved in tumor immunosurveillance in mice. Eur J Immunol. 2020 May;50(5):705-711. doi: 10.1002/eji.201948354. Epub 2020 Mar 1. PMID: 32034922; PMCID: PMC7216943.

11. Davalos D, Grutzendler J, Yang G, Kim JV, Zuo Y, Jung S, Littman DR, Dustin ML, Gan WB. ATP mediates rapid microglial response to local brain injury in vivo. Nat Neurosci. 2005 Jun;8(6):752-8. doi: 10.1038/nn1472. Epub 2005 May 15. PMID: 15895084.

12. Degroote S, Hunting DJ, Baccarelli AA, Takser L. Maternal gut and fetal brain connection: Increased anxiety and reduced social interactions in Wistar rat offspring following peri-conceptional antibiotic exposure. Prog Neuropsychopharmacol Biol Psychiatry. 2016 Nov 3;71:76-82. doi: 10.1016/j.pnpbp.2016.06.010. Epub 2016 Jun 21. PMID: 27346743; PMCID: PMC6584952.

13. Desbonnet L, Clarke G, Traplin A, O'Sullivan O, Crispie F, Moloney RD, Cotter PD, Dinan TG, Cryan JF. Gut microbiota depletion from early adolescence in mice: Implications for brain and behaviour. Brain Behav Immun. 2015 Aug;48:165-73. doi: 10.1016/j.bbi.2015.04.004. Epub 2015 Apr 10. PMID: 25866195.

14. Erny D, Hrabě de Angelis AL, Jaitin D, Wieghofer P, Staszewski O, David E, Keren-Shaul H, Mahlakoiv T, Jakobshagen K, Buch T, Schwierzeck V, Utermöhlen O, Chun E, Garrett WS, McCoy KD, Diefenbach A, Staeheli P, Stecher B, Amit I, Prinz M. Host microbiota constantly control maturation and function of microglia in the CNS. Nat Neurosci. 2015 Jul;18(7):965-77. doi: 10.1038/nn.4030. Epub 2015 Jun 1. PMID: 26030851; PMCID: PMC5528863.

15. Eyo UB, Wu LJ. Bidirectional microglia-neuron communication in the healthy brain. Neural Plast. 2013;2013:456857. doi: 10.1155/2013/456857. Epub 2013 Sep 2. PMID: 24078884; PMCID: PMC3775394.

16. Fond G, Boukouaci W, Chevalier G, Regnault A, Eberl G, Hamdani N, Dickerson F, Macgregor A, Boyer L, Dargel A, Oliveira J, Tamouza R, Leboyer M. The "psychomicrobiotic": Targeting microbiota in major psychiatric disorders: A systematic review. Pathol Biol (Paris). 2015 Feb;63(1):35-42. doi: 10.1016/j.patbio.2014.10.003. Epub 2014 Nov 2. PMID: 25468489.

17. Foster JA, McVey Neufeld KA. Gut-brain axis: how the microbiome influences anxiety and depression. Trends Neurosci. 2013 May;36(5):305-12. doi: 10.1016/j.tins.2013.01.005. Epub 2013 Feb 4. PMID: 23384445.

18. Fröhlich EE, Farzi A, Mayerhofer R, Reichmann F, Jačan A, Wagner B, Zinser E, Bordag N, Magnes C, Fröhlich E, Kashofer K, Gorkiewicz G, Holzer P. Cognitive impairment by antibiotic-induced gut dysbiosis: Analysis of gut microbiota-brain communication. Brain Behav Immun. 2016 Aug;56:140-55. doi: 10.1016/j.bbi.2016.02.020. Epub 2016 Feb 23. PMID: 26923630; PMCID: PMC5014122.

19. Garcez ML, Tan VX, Heng B, Guillemin GJ. Sodium Butyrate and Indole-3-propionic Acid Prevent the Increase of Cytokines and Kynurenine Levels in LPS-induced Human Primary Astrocytes. Int J Tryptophan Res. 2020 Dec 28;13:1178646920978404. doi: 10.1177/1178646920978404. PMID: 33447046; PMCID: PMC7780186.

20. Gyoneva S, Davalos D, Biswas D, Swanger SA, Garnier-Amblard E, Loth F, Akassoglou K, Traynelis SF. Systemic inflammation regulates microglial responses to tissue damage in vivo. Glia. 2014 Aug;62(8):1345-60. doi: 10.1002/glia.22686. Epub 2014 May 7. PMID: 24807189; PMCID: PMC4408916.

21. Guida F, Turco F, Iannotta M, De Gregorio D, Palumbo I, Sarnelli G, Furiano A, Napolitano F, Boccella S, Luongo L, Mazzitelli M, Usiello A, De Filippis F, Iannotti FA, Piscitelli F, Ercolini D, de Novellis V, Di Marzo V, Cuomo R, Maione S. Antibiotic-induced microbiota perturbation causes gut endocannabinoidome changes, hippocampal neuroglial reorganization and depression in mice. Brain Behav Immun. 2018 Jan;67:230-245. doi: 10.1016/j.bbi.2017.09.001. Epub 2017 Sep 7. PMID: 28890155.

22. Hoban AE, Stilling RM, Ryan FJ, Shanahan F, Dinan TG, Claesson MJ, Clarke G, Cryan JF. Regulation of prefrontal cortex myelination by the microbiota. Transl Psychiatry. 2016 Apr 5;6(4):e774. doi: 10.1038/tp.2016.42. PMID: 27045844; PMCID: PMC4872400.

23. Hoshiko M, Arnoux I, Avignone E, Yamamoto N, Audinat E. Deficiency of the microglial receptor CX3CR1 impairs postnatal functional development of thalamocortical synapses in the barrel cortex. J Neurosci. 2012 Oct 24;32(43):15106-11. doi: 10.1523/JNEUROSCI.1167-12.2012. PMID: 23100431; PMCID: PMC6704837.

24. Hsia AY, Malenka RC, Nicoll RA. Development of excitatory circuitry in the hippocampus. J Neurophysiol. 1998 Apr;79(4):2013-24. doi: 10.1152/jn.1998.79.4.2013. PMID: 9535965.

25. Kluge MG, Kracht L, Abdolhoseini M, Ong LK, Johnson SJ, Nilsson M, Walker FR. Impaired microglia process dynamics post-stroke are specific to sites of secondary neurodegeneration. Glia. 2017 Dec;65(12):1885-1899. doi: 10.1002/glia.23201. Epub 2017 Aug 24. PMID: 28836304.

26. Koizumi S, Shigemoto-Mogami Y, Nasu-Tada K, Shinozaki Y, Ohsawa K, Tsuda M, Joshi BV, Jacobson KA, Kohsaka S, Inoue K. UDP acting at P2Y6 receptors is a mediator of microglial phagocytosis. Nature. 2007 Apr 26;446(7139):1091-5. doi: 10.1038/nature05704. Epub 2007 Apr 4. PMID: 17410128; PMCID: PMC3464483.

27. Leclercq S, Mian FM, Stanisz AM, Bindels LB, Cambier E, Ben-Amram H, Koren O, Forsythe P, Bienenstock J. Low-dose penicillin in early life induces long-term changes in murine gut microbiota, brain cytokines and behavior. Nat Commun. 2017 Apr 4;8:15062. doi: 10.1038/ncomms15062. PMID: 28375200; PMCID: PMC5382287.

28. Liddelow SA, Barres BA. Reactive Astrocytes: Production, Function, and Therapeutic Potential. Immunity. 2017 Jun 20;46(6):957-967. doi: 10.1016/j.immuni.2017.06.006. PMID: 28636962.

29. Maggi L, Scianni M, Branchi I, D'Andrea I, Lauro C, Limatola C. CX(3)CR1 deficiency alters hippocampal-dependent plasticity phenomena blunting the effects of enriched environment. Front Cell Neurosci. 2011 Oct 19;5:22. doi: 10.3389/fncel.2011.00022. PMID: 22025910; PMCID: PMC3198035.

30. Marinelli S, Basilico B, Marrone MC, Ragozzino D. Microglia-neuron crosstalk: Signaling mechanism and control of synaptic transmission. Semin Cell Dev Biol. 2019 Oct;94:138-151. doi: 10.1016/j.semcdb.2019.05.017. Epub 2019 May 30. PMID: 31112798.

31. Mezö C, Dokalis N, Mossad O, Staszewski O, Neuber J, Yilmaz B, Schnepf D, de Agüero MG, Ganal-Vonarburg SC, Macpherson AJ, Meyer-Luehmann M, Staeheli P, Blank T, Prinz M, Erny D. Different effects of constitutive and induced microbiota modulation on microglia in a mouse model of Alzheimer's disease. Acta Neuropathol Commun. 2020 Jul 29;8(1):119. doi: 10.1186/s40478-020-00988-5. PMID: 32727612; PMCID: PMC7389451.

32. Möhle L, Mattei D, Heimesaat MM, Bereswill S, Fischer A, Alutis M, French T, Hambardzumyan D, Matzinger P, Dunay IR, Wolf SA. Ly6C(hi) Monocytes Provide a Link between Antibiotic-Induced Changes in Gut Microbiota and Adult Hippocampal Neurogenesis. Cell Rep. 2016 May 31;15(9):1945-56. doi: 10.1016/j.celrep.2016.04.074. Epub 2016 May 19. PMID: 27210745.

33. Nimmerjahn A, Kirchhoff F, Helmchen F. Resting microglial cells are highly dynamic surveillants of brain parenchyma in vivo. Science. 2005 May 27;308(5726):1314-8. doi: 10.1126/science.1110647. Epub 2005 Apr 14. PMID: 15831717.

34. O'Mahony SM, Clarke G, Borre YE, Dinan TG, Cryan JF. Serotonin, tryptophan metabolism and the brain-gut-microbiome axis. Behav Brain Res. 2015 Jan 15;277:32-48. doi: 10.1016/j.bbr.2014.07.027. Epub 2014 Jul 29. PMID: 25078296.

35. Parkhurst, C. N., Yang, G., Ninan, I., Savas, J. N., Yates, J. R., Lafaille, J. J., … Gan, W. B. (2013). Microglia promote learning-dependent synapse formation through brain-derived neurotrophic factor. Cell, 155(7), 1596–1609. doi:10.1016/j.cell.2013.11.030

36. Pagani F, Paolicelli RC, Murana E, Cortese B, Di Angelantonio S, Zurolo E, Guiducci E, Ferreira TA, Garofalo S, Catalano M, D'Alessandro G, Porzia A, Peruzzi G, Mainiero F, Limatola C, Gross CT, Ragozzino D. Defective microglial development in the hippocampus of Cx3cr1 deficient mice. Front Cell Neurosci. 2015 Mar 31;9:111. doi: 10.3389/fncel.2015.00111. PMID: 25873863; PMCID: PMC4379915.

37. Pagani F, Testi C, Grimaldi A, Corsi G, Cortese B, Basilico B, Baiocco P, De Panfilis S, Ragozzino D, Di Angelantonio S. Dimethyl Fumarate Reduces Microglia Functional Response to Tissue Damage and Favors Brain Iron Homeostasis. Neuroscience. 2020 Jul 15;439:241-254. doi: 10.1016/j.neuroscience.2019.10.041. Epub 2019 Nov 15. PMID: 31738884.

38. Paolicelli RC, Bolasco G, Pagani F, Maggi L, Scianni M, Panzanelli P, Giustetto M, Ferreira TA, Guiducci E, Dumas L, Ragozzino D, Gross CT. Synaptic pruning by microglia is necessary for normal brain development. Science. 2011 Sep 9;333(6048):1456-8. doi: 10.1126/science.1202529. Epub 2011 Jul 21. PMID: 21778362.

39. Pfeiffer T, Avignone E, Nägerl UV. Induction of hippocampal long-term potentiation increases the morphological dynamics of microglial processes and prolongs their contacts with dendritic spines. Sci Rep. 2016 Sep 8;6:32422. doi: 10.1038/srep32422. PMID: 27604518; PMCID: PMC5015055.

40. Pusceddu MM, Barboza M, Keogh CE, Schneider M, Stokes P, Sladek JA, Kim HJD, Torres-Fuentes C, Goldfild LR, Gillis SE, Brust-Mascher I, Rabasa G, Wong KA, Lebrilla C, Byndloss MX, Maisonneuve C, Bäumler AJ, Philpott DJ, Ferrero RL, Barrett KE, Reardon C, Gareau MG. Nod-like receptors are critical for gut-brain axis signalling in mice. J Physiol. 2019 Dec;597(24):5777-5797. doi: 10.1113/JP278640. Epub 2019 Nov 27. PMID: 31652348; PMCID: PMC6911019.

41. Schafer DP, Lehrman EK, Kautzman AG, Koyama R, Mardinly AR, Yamasaki R, Ransohoff RM, Greenberg ME, Barres BA, Stevens B. Microglia sculpt postnatal neural circuits in an activity and complement-dependent manner. Neuron. 2012 May 24;74(4):691-705. doi: 10.1016/j.neuron.2012.03.026. PMID: 22632727; PMCID: PMC3528177.

42. Schmittgen TD, Livak KJ. Analyzing real-time PCR data by the comparative C(T) method. Nat Protoc. 2008;3(6):1101-8. doi: 10.1038/nprot.2008.73. PMID: 18546601.

43. Silva YP, Bernardi A, Frozza RL. The Role of Short-Chain Fatty Acids From Gut Microbiota in Gut-Brain Communication. Front Endocrinol (Lausanne). 2020 Jan 31;11:25. doi: 10.3389/fendo.2020.00025. PMID: 32082260; PMCID: PMC7005631.

44. Szepesi Z, Manouchehrian O, Bachiller S, Deierborg T. Bidirectional Microglia-Neuron Communication in Health and Disease. Front Cell Neurosci. 2018 Sep 27;12:323. doi: 10.3389/fncel.2018.00323. PMID: 30319362; PMCID: PMC6170615.

45. Verdú EF, Bercik P, Verma-Gandhu M, Huang XX, Blennerhassett P, Jackson W, Mao Y, Wang L, Rochat F, Collins SM. Specific probiotic therapy attenuates antibiotic induced visceral hypersensitivity in mice. Gut. 2006 Feb;55(2):182-90. doi: 10.1136/gut.2005.066100. Epub 2005 Aug 16. PMID: 16105890; PMCID: PMC1856497.

46. Takayama F, Hayashi Y, Wu Z, Liu Y, Nakanishi H. Diurnal dynamic behavior of microglia in response to infected bacteria through the UDP-P2Y6 receptor system. Sci Rep. 2016 Jul 21;6:30006. doi: 10.1038/srep30006. PMID: 27445174; PMCID: PMC4956748.

47. Tochitani S, Ikeno T, Ito T, Sakurai A, Yamauchi T, Matsuzaki H. Administration of Non-Absorbable Antibiotics to Pregnant Mice to Perturb the Maternal Gut Microbiota Is Associated with Alterations in Offspring Behavior. PLoS One. 2016 Jan 20;11(1):e0138293. doi: 10.1371/journal.pone.0138293. PMID: 26789865; PMCID: PMC4720425.

48. Tremblay MS, Colley RC, Saunders TJ, Healy GN, Owen N. Physiological and health implications of a sedentary lifestyle. Appl Physiol Nutr Metab. 2010 Dec;35(6):725-40. doi: 10.1139/H10-079. PMID: 21164543.

49. Tozaki-Saitoh H, Tsuda M, Inoue K. Role of purinergic receptors in CNS function and neuroprotection. Adv Pharmacol. 2011;61:495-528. doi: 10.1016/B978-0-12-385526-8.00015-1. PMID: 21586368.

50. Wake H, Moorhouse AJ, Jinno S, Kohsaka S, Nabekura J. Resting microglia directly monitor the functional state of synapses in vivo and determine the fate of ischemic terminals. J Neurosci. 2009 Apr 1;29(13):3974-80. doi: 10.1523/JNEUROSCI.4363-08.2009. PMID: 19339593; PMCID: PMC6665392.

51. Weinhard L, di Bartolomei G, Bolasco G, Machado P, Schieber NL, Neniskyte U, Exiga M, Vadisiute A, Raggioli A, Schertel A, Schwab Y, Gross CT. Microglia remodel synapses by presynaptic trogocytosis and spine head filopodia induction. Nat Commun. 2018 Mar 26;9(1):1228. doi: 10.1038/s41467-018-03566-5. PMID: 29581545; PMCID: PMC5964317.

52. Zhan Y, Paolicelli RC, Sforazzini F, Weinhard L, Bolasco G, Pagani F, Vyssotski AL, Bifone A, Gozzi A, Ragozzino D, Gross CT. Deficient neuron-microglia signaling results in impaired functional brain connectivity and social behavior. Nat Neurosci. 2014 Mar;17(3):400-6. doi: 10.1038/nn.3641. Epub 2014 Feb 2. PMID: 24487234.

Clinical trials

Lactobacillus Plantarum PS128 in Patients With Major Depressive Disorder and High Level of Inflammation
ClinicalTrials.gov Identifier: NCT03237078
Prebiotic Intervention for Autism Spectrum Disorders ClinicalTrials.gov Identifier: NCT02720900
Efficacy of Prebiotic and Probiotic Dietary Modulation in Schizophrenic Disorders
ClinicalTrials.gov Identifier: NCT04366401